https://doi.org/10.5194/wes-2026-134
Preprint. Discussion started: 14 August 2026

eawe european academy of wind energy
Open Access WIND ENERGY SCIENCE DISCUSSIONS

Fixed Frame Control-Oriented Modeling and Characterization of Asymmetric Wind Disturbances for Advanced Individual Pitch Control Design

Daniel Lacheta-Lecumberri[1,2], Irene Miquelez-Madariaga[2], and Jorge Elso[2]

[1]Vors Control Technology S.L., Pamplona, Spain
[2]Department of Engineering, Universidad Pública de Navarra, Pamplona, Spain

Correspondence: Daniel Lacheta-Lecumberri (dlacheta@vorscontrol.com)

Abstract. The development of advanced load reduction strategies is becoming increasingly important for modern wind turbines, making it essential to incorporate both the dynamics and the characteristics of the wind disturbances responsible for structural loading into the control design process. In this context, this work proposes a control-oriented framework that combines the modeling and characterization of asymmetric wind disturbances. Starting from a linearized model with distributed horizontal wind inputs, the inflow is reduced to three equivalent disturbances in a fixed reference frame through a sensitivity-based aggregation of the wind field. The methodology is validated on the IEA 15 MW Reference Wind Turbine, including all relevant aeroelastic degrees of freedom, through turbulent OpenFAST simulations. The results demonstrate accurate reconstruction of open-loop time-domain responses and prediction of closed-loop output spectra, enabling control design to be directly focused on the disturbances to be rejected while reducing the reliance on computationally expensive aeroelastic simulations.

1 Introduction

The continuous growth of wind turbine size has been one of the main drivers of the reduction in the cost of wind energy. In particular, the increase in rotor diameter has enabled higher energy capture by enlarging the swept area (Henrique et al., 2025). However, large rotors are exposed to greater spatial variability in the wind field, leading to an increase in structural loads (Trigaux et al., 2024; Canet et al., 2021). As a result, advanced control strategies have become increasingly important for modern large-scale wind turbines, not only to ensure efficient power regulation but also to mitigate the structural loads arising from complex aerodynamic excitation (Bošnjaković et al., 2022).

Despite the distributed nature of the aerodynamic interaction, wind turbine control design is commonly based on lumped linear models. In these models, the inflow disturbance is typically represented by an equivalent wind disturbance which represents the homogeneous horizontal wind speed acting on the rotor (Jonkman et al., 2018). In this context, the characterization of the equivalent wind disturbance is essential, since the resulting controller is designed according to the effect of this input on the turbine response.

https://doi.org/10.5194/wes-2026-134
Preprint. Discussion started: 14 August 2026

The most widely adopted representation of this equivalent disturbance is the Rotor Effective Wind Speed (REWS) (Schlipf, 2008). Since collective variables such as rotor speed or generated power are mainly driven by the overall aerodynamic behaviour of the rotor, REWS provides a suitable representation of the inflow for many control-oriented applications. Accordingly, it has been extensively used in wind turbine control design, specially in LIDAR-assisted control strategies (see e.g., (Schlipf et al., 2013; Miquelez-Madariaga et al., 2022; Miquelez-Madariaga et al., 2023)). For control objectives involving collective variables, the combination of REWS disturbance characterization and conventional lumped models is generally sufficient. However, when the response of interest is primarily driven by asymmetric inflow effects, a single collective disturbance is not enough to capture the spatial variability of the aerodynamic excitation across the rotor plane.

To overcome this limitation, several alternative inflow representations have been proposed in the literature. Among them, Blade Effective Wind Speed (BEWS) formulations have been introduced to provide additional information about the aerodynamic conditions experienced by each blade (Simley and Pao, 2013). Other works have addressed the estimation of physically meaningful asymmetric inflow variables, such as wind shear, wind misalignment or upflow angle, from turbine measurements and load signals (Bottasso et al., 2018; Cacciola et al., 2016; Bertelè et al., 2017, 2024). These approaches provide information about the spatial variability of the wind field and enable the characterization of asymmetric inflow phenomena. However, their primary focus remains the estimation and characterization of the disturbances themselves, rather than the development of control-oriented models describing their effect on the turbine response.

In parallel, several control-oriented wind turbine models incorporating asymmetric aerodynamic effects have also been proposed. Since the individual pitch control (IPC) is the most commonly adopted strategy for asymmetric load alleviation (Burton et al., 2021), the vast majority of studies focus on it. For example, Selvam et al. (2009), Laks et al. (2010) and Tang et al. (2022) account for asymmetric inflow effects by introducing blade-specific wind speed disturbances, where the aerodynamic excitation of each blade is represented by an individual wind speed input. Alternatively, in Yuan et al. (2020), the aerodynamic disturbances are described through horizontal and vertical wind shear components. Nevertheless, the associated disturbances are typically introduced as model inputs without an accompanying temporal or spectral characterization. As a result, the relationship between the disturbance characteristics and the corresponding turbine response remains difficult to analyze within a unified control-oriented framework.

Consequently, although asymmetric disturbance characterization and control-oriented modeling have both been addressed separately in the literature, a unified framework combining equivalent asymmetric inflow disturbance modeling and their characterization for advanced control-oriented applications is still missing. As a result, the design of advanced asymmetric load reduction strategies, such as IPC, is typically carried out by considering only the dynamic relationship between the blade pitch inputs and the controlled loads, while the disturbances responsible for exciting those loads are not explicitly incorporated into the design process (see e.g. (Lara et al., 2025; Hummel et al., 2025)).

To address this gap, this work proposes a unified control-oriented framework based on equivalent wind disturbances in the *0dq* reference frame. This formulation exploits the Multi-Blade Coordinate (MBC) transformation (Park, 1929), which provides a fixed-frame representation of asymmetric rotor quantities and constitutes the basis of conventional IPC implementations (Bossanyi, 2003). Within this framework, an enriched lumped disturbance model is derived by post-processing the linearized

https://doi.org/10.5194/wes-2026-134
Preprint. Discussion started: 14 August 2026

models routinely provided by aeroelastic simulation tools used in wind turbine control design. The distributed inflow is thereby reduced to three equivalent disturbance channels, associated with the collective, tilt and yaw inflow components, which are subsequently characterized in time and frequency domains to support advanced asymmetric load reduction strategies.

As a result, the proposed framework enables the systematic design of asymmetric load reduction strategies by explicitly incorporating both the model and the characterization of the disturbances affecting the system. In this way, the control design effort can be rigorously linked to the characteristics of the disturbances to be rejected, leading to a more transparent and consistent control design workflow. Moreover, the framework enables the prediction of the spectral response of controlled wind turbine signals directly from the linear model, facilitating the comparison and assessment of different control designs, the evaluation of disturbance-rejection capabilities, and the formulation of frequency-domain design specifications. This provides an efficient basis for advanced control-oriented analyses while reducing the need for computationally expensive aeroelastic time-domain simulations during the controller design process.

The remainder of the paper is organized as follows. Section 2 reviews the theoretical background on linear wind turbine modeling, the MBC transformation and the conventional IPC design. Section 3 presents the proposed equivalent disturbance framework, including the distributed wind input formulation and its reduction to three equivalent disturbances. Section 4 validates the proposed methodology through time domain simulations and spectral analyses under different closed-loop configurations. Finally, Section 5 summarizes the conclusions and future work.

2 Theoretical Background

This section introduces the theoretical tools on which the proposed framework is built. The linearization of the nonlinear aeroelastic wind turbine model is first reviewed to establish the linear state-space model used throughout the paper. The Multi-Blade Coordinate (MBC) transformation is then briefly presented as the standard approach for mapping rotating quantities into a fixed *0dq* reference frame, enabling time-invariant control-oriented models. Finally, the conventional Individual Pitch Control (IPC) strategy is summarized, as it provides the baseline asymmetric load reduction framework used later for validation.

2.1 Linear wind turbine modeling

Let us consider the wind turbine equations of motion, expressed in state-space form as

$$\dot{\mathbf{x}}(t) = f\left(\mathbf{x}(t), \mathbf{u}(t), \mathbf{w}(t)\right), \qquad \mathbf{y}(t) = g\left(\mathbf{x}(t), \mathbf{u}(t), \mathbf{w}(t)\right), \tag{1}$$

where $\mathbf{x} \in \mathbb{R}^{n\times 1}$ is the state vector, $\mathbf{u} \in \mathbb{R}^{m\times 1}$ is the vector of inputs to the system, $\mathbf{w} \in \mathbb{R}^{p\times 1}$ is the vector of disturbances of the system and $\mathbf{y} \in \mathbb{R}^{q\times 1}$ is the vector of outputs.

The nonlinear model is linearized around a steady operating condition. Since the rotor is spinning, the steady-state solution and the correspondng linearized dynamics are periodic with the rotor azimuth angle ψ. Therefore, the linearization is performed at several azimuth positions ψ_k over one rotor revolution.

https://doi.org/10.5194/wes-2026-134
Preprint. Discussion started: 14 August 2026

Around each operating point, the variables are written as deviations from their steady-state values as: $\mathbf{x} = \mathbf{x}_{op} + \delta\mathbf{x}$, leading to the first-order linear model

$$\begin{cases} \delta\dot{\mathbf{x}} = \mathbf{A}(\psi_k)\delta\mathbf{x} + \mathbf{B}(\psi_k)\delta\mathbf{u} + \mathbf{B}_w(\psi_k)\delta\mathbf{w} \\ \delta\mathbf{y} = \mathbf{C}(\psi_k)\delta\mathbf{x} + \mathbf{D}(\psi_k)\delta\mathbf{u} + \mathbf{D}_w(\psi_k)\delta\mathbf{w} \end{cases} \tag{2}$$

where the system matrices $\mathbf{A}$, $\mathbf{B}$, $\mathbf{B}_w$, $\mathbf{C}$, $\mathbf{D}$ and $\mathbf{D}_w$ are the Jacobians of f and g evaluated at the corresponding azimuth-dependent operating point.

The result of the linearization is a periodic model consisting of a family of linear models describing the local input-output behavior of the wind turbine around the selected operating point. Although these models provide the basis for linear control-oriented analysis, their explicit azimuth dependence prevents their direct use as standard linear time-invariant (LTI) representations. The MBC transformation, introduced in the next subsection, is commonly used to project rotating quantities into a fixed reference frame and obtain models suitable for conventional control design.

2.2 Multi-blade coordinate transformation

As discussed in the previous subsection, the linearized wind turbine model depends periodically on the rotor azimuth angle. This periodicity arises from the interaction between rotating components, such as the blades, and non-rotating components, such as the tower, for example. As a result, the state-space matrices obtained at different azimuth positions cannot be directly averaged while relevant state, input or output signals remain expressed in the rotating frame (Stol et al., 2009).

The Multi-Blade Coordinate (MBC) transformation $T(\psi(t))$ provides a standard procedure to express three-bladed rotating quantities in a fixed reference frame (Park, 1929). Given a generic rotating signal $\mathbf{y}_{123}(t) = [y_1(t), y_2(t), y_3(t)]^\top$, the transformation into collective (*0*), tilt (d) and yaw (q) axis is defined as

$$\begin{bmatrix} y_0(t) \\ y_d(t) \\ y_q(t) \end{bmatrix} = \underbrace{\frac{2}{3}\begin{bmatrix} 1/2 & 1/2 & 1/2 \\ \cos(\psi(t)) & \cos\left(\psi(t)+\frac{2\pi}{3}\right) & \cos\left(\psi(t)+\frac{4\pi}{3}\right) \\ \sin(\psi(t)) & \sin\left(\psi(t)+\frac{2\pi}{3}\right) & \sin\left(\psi(t)+\frac{4\pi}{3}\right) \end{bmatrix}}_{T(\psi(t))} \begin{bmatrix} y_1(t) \\ y_2(t) \\ y_3(t) \end{bmatrix}. \tag{3}$$

The *0* component represents the collective contribution, while the d and q components describe asymmetric contributions associated with the tilt and yaw directions, respectively.

Similarly, the inverse transformation $T^{-1}(\psi(t))$ maps non-rotating quantities back to the rotating frame as

$$\begin{bmatrix} y_1(t) \\ y_2(t) \\ y_3(t) \end{bmatrix} = \underbrace{\begin{bmatrix} 1 & \cos(\psi(t)) & \sin(\psi(t)) \\ 1 & \cos\left(\psi(t)+\frac{2\pi}{3}\right) & \sin\left(\psi(t)+\frac{2\pi}{3}\right) \\ 1 & \cos\left(\psi(t)+\frac{4\pi}{3}\right) & \sin\left(\psi(t)+\frac{4\pi}{3}\right) \end{bmatrix}}_{T^{-1}(\psi(t))} \begin{bmatrix} y_0(t) \\ y_d(t) \\ y_q(t) \end{bmatrix}. \tag{4}$$

The MBC transformation can be applied directly to the azimuth dependent set of state space models obtained from the linearization process. By applying this transformation to rotating states, inputs and outputs, the dominant azimuth-dependent

https://doi.org/10.5194/wes-2026-134
Preprint. Discussion started: 14 August 2026

terms of the linearized model are removed or significantly reduced (Bir, 2008). The transformed system matrices can then be consistently averaged over one rotor revolution, leading to a single linear time-invariant representation of the form

$$\begin{cases} \delta\dot{\mathbf{x}}_{0dq} = \bar{\mathbf{A}}_{0dq}\delta\mathbf{x}_{0dq} + \bar{\mathbf{B}}_{0dq}\delta\mathbf{u}_{0dq} + \bar{\mathbf{B}}_{w,0dq}\delta\mathbf{w}_{0dq}, \\ \delta\mathbf{y}_{0dq} = \bar{\mathbf{C}}_{0dq}\delta\mathbf{x}_{0dq} + \bar{\mathbf{D}}_{0dq}\delta\mathbf{u}_{0dq} + \bar{\mathbf{D}}_{w,0dq}\delta\mathbf{w}_{0dq}. \end{cases} \quad (5)$$

This fixed-frame representation is particularly useful for wind turbine control, since periodic blade loads can be expressed as nearly stationary quantities in the *dq* frame. This principle is exploited in conventional Individual Pitch Control (IPC) strategy, which is briefly reviewed in the following subsection.

2.3 Conventional IPC framework

Individual Pitch Control (IPC) is a well-known control strategy aimed at mitigating periodic structural loads. Unlike collective pitch control, which applies the same pitch command to all blades, IPC generates an specific pitch variation for each blade to counteract asymmetric aerodynamic loading (Burton et al., 2021). This is particularly important in large-scale wind turbines where spatial variations in the wind field lead to significant periodic loads, primarily at once-per-revolution and higher harmonic frequencies (nP) (Dai et al., 2022).

The primary objective of traditional IPC strategies is to reduce out-of-plane (OoP) blade vibrations. As mentioned in the previous subsection, classical implementations use the Multi-Blade Coordinate (MBC) transformation to express the OoP bending moments of each blade M_{123} from the rotating frame to the fixed (non-rotating) frame, following the Equation (3). In this way, the resulting signals M_{0dq} can be interpreted as virtual moments associated with the collective, tilt and yaw motions of the rotor, as depicted in Figure 1. The periodic blade loads that appear at 1P in the rotating frame are therefore respresented as low-frequency signals in the *0dq* frame, which enables the use of simple linear control laws (Bossanyi, 2003).

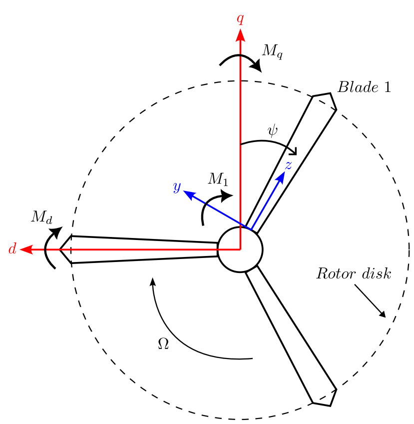

Figure 1. Definition of the blade rotating frame (blue) and the rotor fixed frame (red).

The usual IPC objective is to reject these asymmetric load components by regulating $M_{d,q}$ towards zero, while the collective component M_0 is typically not used for IPC action. The controller generates virtual pitch commands in the fixed frame $\beta_{d,q}$,

https://doi.org/10.5194/wes-2026-134
Preprint. Discussion started: 14 August 2026

which are transformed back to individual blade pitch references through the inverse MBC transformation (Equation (4)), where β_0 denotes the collective pitch contribution, usually provided by the rotor speed loop.

135 This conventional architecture is summarized in Figure 2 in the Laplace domain, where $P_{0dq}(s)$ denotes the wind turbine plant expressed in the fixed reference frame. The diagram highlights that IPC is designed from the pitch-to-load dynamics and the measured asymmetric outputs. However, the disturbances responsible for exciting these signals are not explicitly represented. This is precisely the enhancement that this work proposes: a design framework in which the disturbances that the IPC loop must face are accurately described and, consequently, more easily tackled.

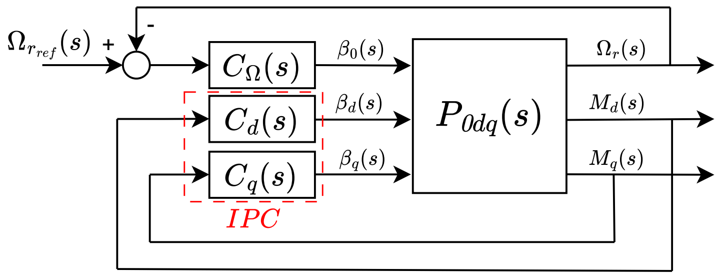

Figure 2. Block diagram used for the control baseline design.

140 This conventional IPC framework provides the control-oriented context for the present work, in which asymmetric loads are naturally handled in the fixed frame. The following section addresses the lack of an explicit disturbance representation by introducing a framework that models and characterizes the disturbances exciting these channels.

3 Equivalent Disturbance Framework

To address the need for modeling and characterizing the asymmetric disturbances affecting the system, this section introduces
145 the proposed equivalent disturbance framework. The disturbance input vector of the linearized model is augmented with blade-node horizontal wind disturbances and subsequently reduced, through a sensitivity-based formulation, to three equivalent disturbances in the fixed *0dq* frame suitable for control-oriented analysis and design.

3.1 Distributed horizontal wind input

Let u_b^n denote the horizontal wind speed at blade $b \in \{1,2,3\}$ and node $n \in \{1,\ldots,N\}$, where each node corresponds to a
150 discrete blade-element location along the blade span. The distributed horizontal wind disturbance vector $\delta\mathbf{w}_{dist,123}$ is then constructed as

$$\delta\mathbf{w}_{dist,123} = [\delta u_1^1, \quad \ldots, \quad \delta u_1^N, \quad \delta u_2^1, \quad \ldots, \quad \delta u_2^N, \quad \delta u_3^1, \quad \ldots, \quad \delta u_3^N]^\top. \tag{6}$$

The resulting state-space model integrates the relationship between the outputs of the system with the nodal horizontal undisturbed wind of each blade.

https://doi.org/10.5194/wes-2026-134
Preprint. Discussion started: 14 August 2026

WIND ENERGY SCIENCE DISCUSSIONS

Although this formulation preserves the distributed nature of the wind field, the resulting disturbance vector is high-dimensional and expressed in the rotating blade frame. Following the state-space MBC formulation (Bir, 2008), the transformation is applied similarly to the distributed disturbance input. In this way, the blade-frame nodal wind disturbances are expressed in the fixed *0dq* frame, yielding an equivalent disturbance input vector composed of collective, tilt and yaw horizontal wind components at each radial position. The transformed disturbance vector is defined as

$$\delta \mathbf{w}_{dist,0dq} = [\delta u_0^1, \quad \ldots, \quad \delta u_0^N, \quad \delta u_d^1, \quad \ldots, \quad \delta u_d^N, \quad \delta u_q^1, \quad \ldots, \quad \delta u_q^N]^\top. \tag{7}$$

After applying the MBC transformation to the azimuth-dependent state-space model and averaging the transformed matrices over one rotor revolution, the augmented fixed-frame LTI representation is defined as

$$\begin{cases} \delta \dot{\mathbf{x}}_{0dq} = \bar{\mathbf{A}}_{0dq} \delta \mathbf{x}_{0dq} + \bar{\mathbf{B}}_{0dq} \delta \mathbf{u}_{0dq} + \bar{\mathbf{B}}_{w,0dq} \delta \mathbf{w}_{dist,0dq}, \\ \delta \mathbf{y}_{0dq} = \bar{\mathbf{C}}_{0dq} \delta \mathbf{x}_{0dq} + \bar{\mathbf{D}}_{0dq} \delta \mathbf{u}_{0dq} + \bar{\mathbf{D}}_{w,0dq} \delta \mathbf{w}_{dist,0dq}. \end{cases} \tag{8}$$

In this model, the distributed wind disturbance is represented by $3N$ fixed-frame input channels, corresponding to collective, tilt and yaw wind components at each radial node. Although this representation preserves the spatial structure of the inflow and enables the computation of fixed-frame input-output sensitivities, its high dimensionality makes it unsuitable for direct disturbance characterization and control-oriented analysis, motivating the reduced equivalent disturbance formulation introduced in the following subsection.

3.2 Equivalent disturbance definition

To address the high dimensionality of the distributed wind input, a reduced-order disturbance representation is proposed. The key idea is to replace the distributed wind inputs by a minimal set of equivalent disturbance channels defined in the *0dq* reference frame. These equivalent disturbances are built such that they preserve the input-output behaviour of the system with respect to selected outputs, while enabling a low-dimensional and physically interpretable description of the inflow.

Accordingly, one equivalent disturbance is defined for each component of the fixed *0dq* reference frame, yielding three disturbance channels associated with the collective, tilt and yaw inflow components. These disturbances are denoted as δW_0^{eq}, δW_d^{eq} and δW_q^{eq}, respectively. This leads to a reduced LTI representation of the form

$$\delta Y(s) = G_{y,0}^{eq}(s) \delta W_0^{eq}(s) + G_{y,d}^{eq}(s) \delta W_d^{eq}(s) + G_{y,q}^{eq}(s) \delta W_q^{eq}(s), \tag{9}$$

where $G_{y,i}^{eq}(s)$, with $i \in \{0, d, q\}$, denotes the equivalent transfer function from the corresponding equivalent disturbance to the output y.

The equivalent disturbance signals are defined by exploiting the linear superposition property of the LTI model and the spatial distribution of the input-output sensitivities, defined as the gains between the distributed wind inputs and the selected output. For a given output $y(t)$, the contribution of the distributed wind inputs in a given *0dq* channel (e.g. the d axis) can be expressed as

$$\delta y_d(t) = \sum_{n=1}^{N} g_{y,u_d}^n(t) * \delta u_d^n(t), \tag{10}$$

https://doi.org/10.5194/wes-2026-134
Preprint. Discussion started: 14 August 2026

where $g^n_{y,u_d}(t)$ denotes the impulse response of the transfer function from the wind disturbance $\delta u^n_d(t)$ at radial position n to the output $y(t)$. This expression highlights that the system response results from the weighted contribution of all radial elements, as determined by their respective input-output sensitivities.

The equivalent disturbance δW^{eq}_d is then defined such that the same input-output mapping is preserved in a reduced order form as

$$\delta y_d(t) = g^{eq}_{y,d}(t) * \delta W^{eq}_d(t), \tag{11}$$

where $g^{eq}_d(t)$ is the impulse response of the transfer function given by

$$G^{eq}_{y,d}(s) = \sum_{n=1}^{N} G^n_{y,d}(s). \tag{12}$$

This leads to the following definition of the equivalent disturbance:

$$\delta W^{eq}_d(t) = \frac{\sum_{n=1}^{N} G^n_{y,d}(0)\delta u^n_d(t)}{\sum_{n=1}^{N} G^n_{y,d}(0)}, \tag{13}$$

being $G(0)$ the static gains of the selected transfer functions. Analogous expressions are obtained for the collective $\delta W^{eq}_0(t)$ and yaw components $\delta W^{eq}_q(t)$.

In this way, the term $\delta W^{eq}_{0,d,q}(t)$ represents a reduced order description of the distributed inflow in the *0dq* axis, built so that it reproduces the same system response as the full set of nodal wind disturbances when propagated through the linear model. In this sense, the equivalent disturbance can be interpreted as a projection of the spatially distributed wind field onto a single control relevant coordinate.

The formulation shows that the equivalent disturbances are obtained through a sensitivity weighted aggregation of the distributed wind inputs. The weighting factors are directly determined by the static input-output sensitivities of the system $G(0)$, such that rotor regions with higher influence on the selected output contribute more strongly to the equivalent disturbance. The use of static gains in this definition ensures that the dynamic characteristics of the wind signal are preserved, while the system dynamics are subsequent captured through the equivalent dynamic model $G^{eq}_{y,i}(s)$.

The construction of the equivalent disturbances requires the selection of a reference output to define the sensitivity weights. Therefore, the resulting disturbances are, in principle, output-dependent. In practice, physically meaningful output pairings are selected for each *0dq* channel, such as a collective response for δW^{eq}_0 and fixed-frame asymmetric load components for δW^{eq}_d and δW^{eq}_q. These canonical pairings provide a physically consistent definition of the equivalent disturbance channels, as each set of sensitivity weights is derived from an output directly associated with the corresponding inflow component. The performance of the resulting reduced-order formulation is assessed in the validation section.

4 Validation

Once the methodology has been defined, the objective is to assess its capability to represent the wind turbine response using the reduced order linear model. This section presents the validation of the framework through high-fidelity aeroelastic simulations.

https://doi.org/10.5194/wes-2026-134
Preprint. Discussion started: 14 August 2026

eawe european academy of wind energy
Open Access WIND ENERGY SCIENCE DISCUSSIONS

First, the simulation setup is described. Then, the equivalent disturbances are characterized and their robustness with respect to the selected reference output is assessed. Subsequently, the reduced-order model is validated in the open-loop time domain. Finally, the characterized disturbance spectra are propagated through the closed-loop transfer functions to assess the ability of the proposed framework to predict the output PSDs under different control configurations.

4.1 Simulation setup

The proposed method is validated using the IEA 15 MW Reference Wind Turbine in its offshore monopile configuration (Gaertner et al., 2020), with rated power 15 MW, rotor diameter 240 m and hub height 150 m. The turbine is modeled and simulated in OpenFAST (Jonkman and Buhl, 2005), which is also used to obtain the linearized models required for the equivalent disturbance formulation. To capture the dominant aeroelastic couplings for simulation and control design, the model incorporates the following degrees of freedom (DOFs):

- **Blades**: First and second flapwise bending modes and first edgewise bending mode of each blade.
- **Tower**: First and second fore-aft and side-side bending moments.
- **Nacelle and Drivetrain**: Yaw motion and generator rotation.
- **Foundation**: Translational and rotational motions of the support structure.

The selected operating point (OP) corresponds to above-rated operation at a mean wind speed of 19 m/s, with vertical shear coefficient 0.2, blade pitch angle 16.5 deg and rated generator torque. The linear model is obtained around this OP from 36 azimuth-dependent state space linear models, computed every 10 degrees over one rotor revolution. For the distributed wind formulation, the horizontal wind disturbance is defined at $N = 50$ nodes per blade, resulting in an augmented disturbance vector of $3N = 150$ elements before the equivalent disturbance reduction.

Time-domain aeroelastic simulations are carried out in OpenFAST using turbulent wind fields generated with TurbSim (Jonkman, 2009). Ten independent turbulent wind seeds are considered, each with a duration of 3600s, following IEC class B Normal Turbulence Model conditions based on the Kaimal spectrum (IEC Technical Committee, 2020). For the closed-loop simulations, control algorithms are implemented through the MATLAB/Simulink interface. Hydrodynamic excitation is neglected by considering still water conditions.

4.2 Equivalent disturbances characterization

This subsection characterizes the equivalent disturbances obtained for the considered case study before using them for response reconstruction and spectral propagation. First, their time-domain behavior and open-loop power spectral densities are analyzed from turbulent wind simulations. Then, their dependence on the selected reference output is assessed to verify the consistency of the canonical input-output pairings adopted in the following validation steps.

https://doi.org/10.5194/wes-2026-134
Preprint. Discussion started: 14 August 2026

4.2.1 Temporal and spectral characterization

The equivalent disturbances are first computed from open-loop turbulent simulations using the methodology proposed in Section 3.2. For each equivalent *0dq* disturbance, the sensitivity weights are obtained from physically aligned reference outputs. Rotor speed Ω_r is used for the collective disturbance $\delta W_0^{eq}(t)$, while the tilt and yaw moments, M_d and M_q, obtained from the blade root bending moments, are used for $\delta W_d^{eq}(t)$ and $\delta W_q^{eq}(t)$, respectively.

Figure 3 depicts the corresponding normalized sensitivity distributions along the rotor span. These distributions represent the relative contribution of each radial position to the equivalent disturbance definition. For the collective *0* channel, the sensitivity associated with Ω_r remains relatively uniform over most of the blade span, indicating that rotor speed is mainly influenced by the overall collective inflow across the rotor. In contrast, the asymmetric channels exhibit a stronger contribution from the outer rotor sections, reflecting the increasing aerodynamic leverage of these regions on the tilt and yaw moments. Moreover, due to the rotor symmetry, they appear practically superimposed.

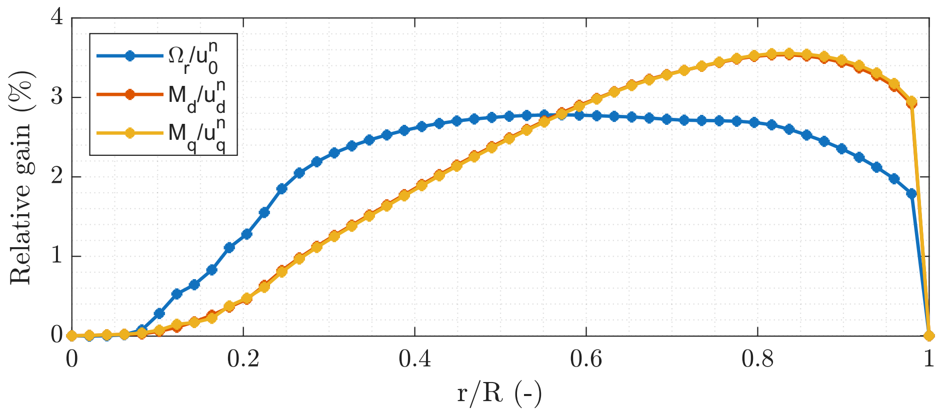

Figure 3. Normalized radial sensitivity distributions used to define the equivalent collective (blue), tilt (red) and yaw (yellow) disturbances. The gain at each radial position is expressed as a percentage of the total equivalent gain.

For each turbulent seed, the undisturbed horizontal wind speed at each blade node are extracted and processed to obtain the corresponding fixed-frame components $u_{0dq}^n(t)$. To avoid inconsistencies with the treatment of linear models, their mean values, associated with the OP, are removed before applying the reduction methodology proposed.

Once the radial sensitivity weights and the corresponding time-domain wind signals $u_{0dq}^n(t)$ have been defined, the equivalent disturbances $\delta W_0^{eq}(t)$, $\delta W_d^{eq}(t)$ and $\delta W_q^{eq}(t)$ are computed from Equation (13).

Figure 4 shows a representative time-domain realization of the equivalent disturbances. The blue lines represent the instantaneous equivalent disturbances, while the red lines show a moving-average filtered version of the same signals, included for visualization purposes to highlight their underlying trends. Note that all three signals represent disturbances with respect to the operating point and therefore oscillate around zero.

https://doi.org/10.5194/wes-2026-134
Preprint. Discussion started: 14 August 2026

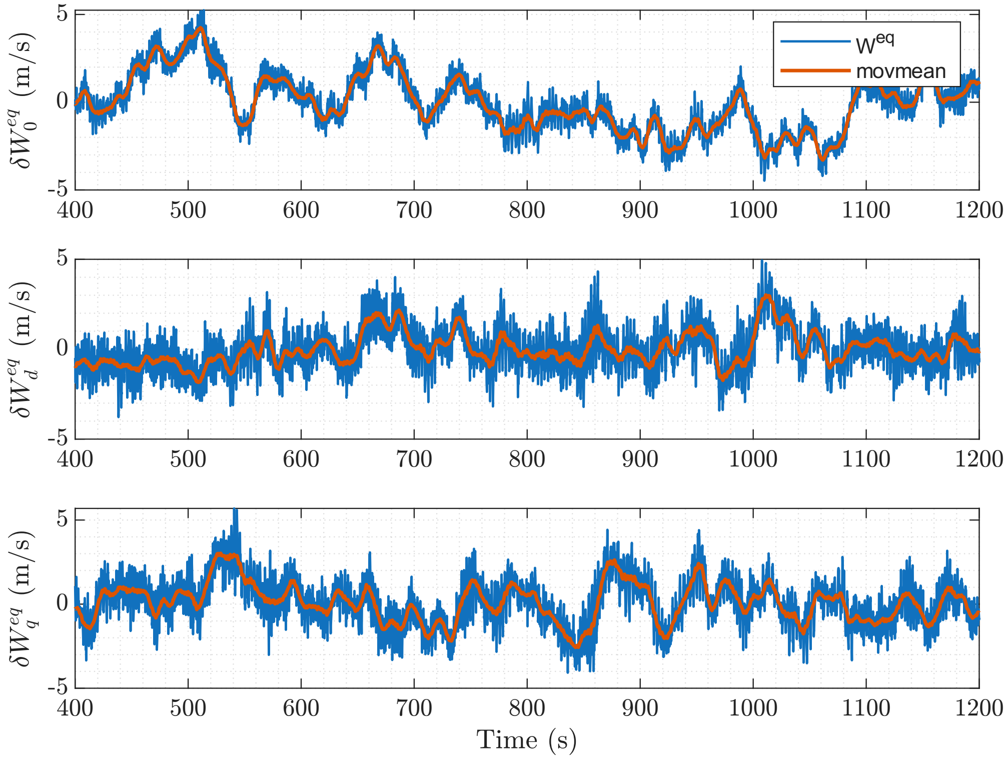

Figure 4. Equivalent wind disturbances in the *0dq* frame. Blue lines show instantaneous signals, while red lines indicate moving-average trends.

The Power Spectral Densities (PSDs) of the equivalent disturbances are estimated from the open-loop turbulent simulations using Welch's method and averaged over the ten wind seeds. The resulting spectra, shown in Figure 5, provide the frequency domain characterization of the *0dq* equivalent disturbances used later for the closed-loop spectral propagation. The collective component exhibits the largest low-frequency content, whereas the *dq* components show very similar spectral levels due to the symmetry of the rotor.

Since the nodal wind velocities are obtained at blade positions that are rotating with the rotor, the equivalent disturbances inherently contain forced periodic components associated with the rotational sampling of the wind field. These components appear as harmonics of the rotor frecuency *nP* in the blade frame. After the MBC transformation, these components appear at multiples of *3nP*. Consequently, the temporal signals exhibit the high-frequency ripple visible in Figure 4, while distinct spectral peaks can be observed around the *3P* and *6P* frequencies in Figure 5.

4.2.2 Output invariance assessment

Since the equivalent disturbance weights are defined from input-output sensitivities, the resulting signals may depend on the selected reference output. To assess this dependence, the equivalent disturbances are computed using four different outputs:

https://doi.org/10.5194/wes-2026-134
Preprint. Discussion started: 14 August 2026

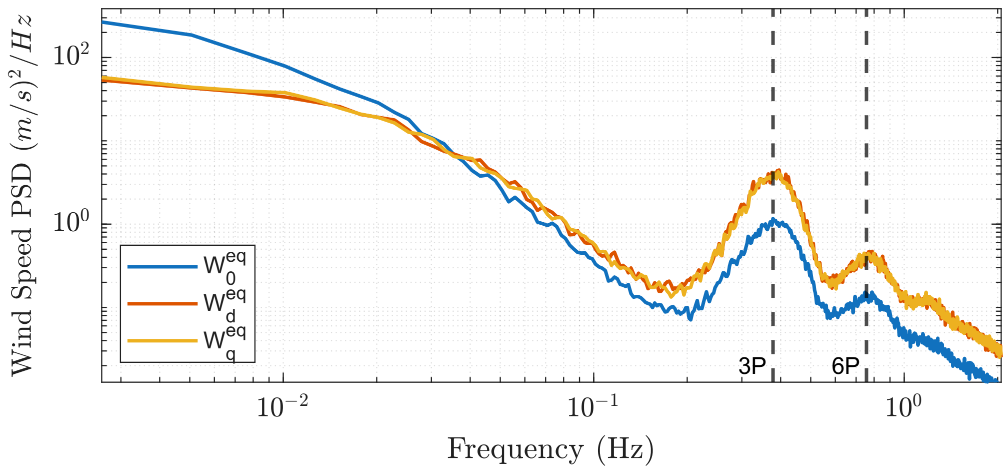

Figure 5. Power spectral densities of the equivalent wind disturbances in the *0dq* reference frame, obtained from turbulent open loop simulations.

rotor speed (Ω_r), tilt moment (M_d), yaw moment (M_q) and tower base bending moment (*TwrMy*). The resulting time series are compared in Figure 6.

The results show that the equivalent disturbances obtained from different reference outputs are highly consistent, with the corresponding time series being almost superimposed for each *0dq* channel. This indicates that the proposed methodology captures dominant collective and asymmetric inflow components that are largely independent of the particular output used for their construction.

Small deviations observed are mainly associated with reference outputs whose radial sensitivity distributions present sign changes along the rotor span, leading to partial cancellations in the weighted aggregation. Therefore, based on this analysis, the canonical input-output pairings, defined in the previous subsection, are adopted for the remainder of the validation.

4.3 Open-loop time-domain validation

The time-domain validation assesses the ability of the proposed reduced-order linear model to reproduce the turbine response under open-loop turbulent conditions. For each wind realization, the three equivalent disturbances $\{\delta W_0^{eq}(t), \delta W_d^{eq}(t), \delta W_q^{eq}(t)\}$ are computed from OpenFAST $u_{0dq}^n(t)$ measurements and used as inputs to the equivalent LTI model. The reconstructed output $\delta\hat{y}(t)$ is obtained as

$$\delta\hat{y}(t) = g_{y,0}^{eq}(t) * \delta W_0^{eq}(t) + g_{y,d}^{eq}(t) * \delta W_d^{eq}(t) + g_{y,q}^{eq}(t) * \delta W_q^{eq}(t). \tag{14}$$

The outputs are also reconstructed using the conventional Rotor Effective Wind Speed (REWS) representation, defined as the horizontal wind speed averaged over the rotor disk (Schlipf et al., 2013). In this case, the standard linear model is employed, where REWS constitutes the single disturbance input of the system (Jonkman et al., 2018). This provides a benchmark to assess the benefits of explicitly incorporating asymmetric disturbance channels into the model.

https://doi.org/10.5194/wes-2026-134
Preprint. Discussion started: 14 August 2026

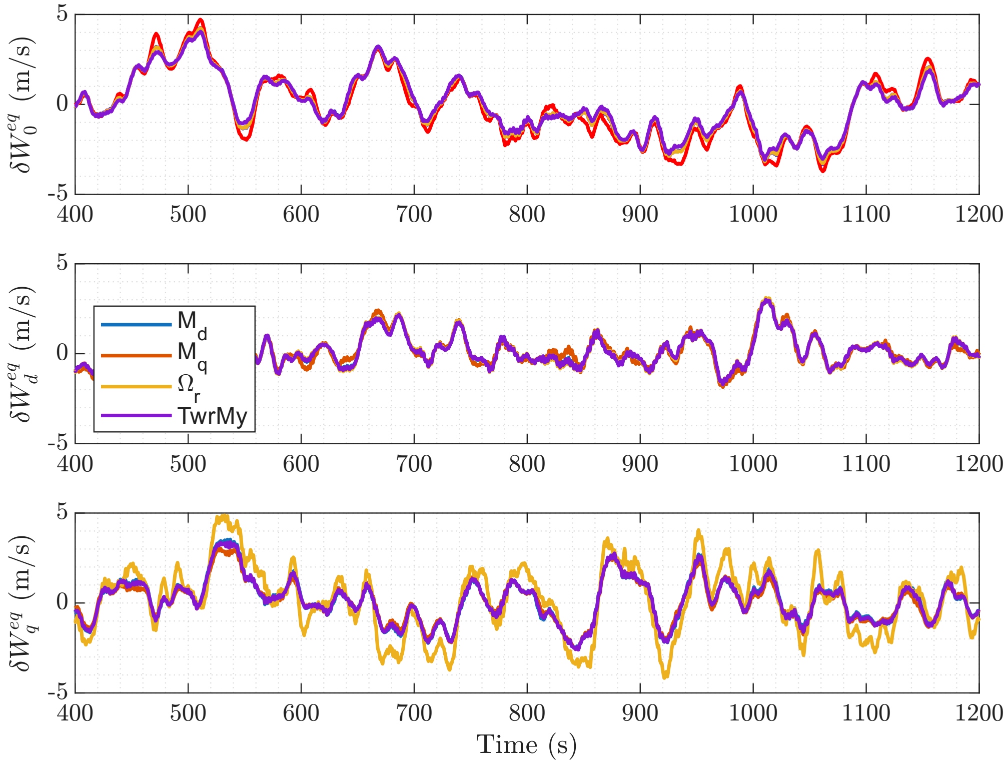

Figure 6. Equivalent wind disturbances in the *0dq* frame characterized from four different system outputs.

The reconstructed signals are compared with the corresponding outputs obtained from nonlinear OpenFAST simulations. The selected outputs are rotor speed Ω_r, tilt moment M_d, yaw moment M_q and tower-base bending moment *TwrMy*, which provide a representative set of collective and asymmetric responses relevant for control design.

Figure 7 compares the simulated responses with those reconstructed using the proposed equivalent disturbance framework and the conventional REWS-based representation. The proposed framework reproduces the main features of all considered outputs, showing a close agreement with the nonlinear simulations. The REWS-based reconstruction also captures the dominant trends of outputs mainly influenced by the collective inflow, such as rotor speed Ω_r and, to some extent, the tower-base bending moment *TwrMy*. However, as expected, it is unable to reproduce the asymmetric responses represented by the tilt and yaw moments M_d and M_q.

A quantitative assessment is performed over the ten turbulent wind realizations using the coefficient of determination, R^2, and the normalized root mean square error, *NRMSE*, defined as

$$R^2 = 1 - \frac{\sum_{i=1}^{K}(y_i - \hat{y}_i)^2}{\sum_{i=1}^{K}(y_i - \bar{y})^2}, \qquad NRMSE(\%) = \frac{100}{y_{max} - y_{min}} \sqrt{\frac{1}{K}\sum_{i=1}^{K}(y_i - \hat{y}_i)^2}. \tag{15}$$

https://doi.org/10.5194/wes-2026-134
Preprint. Discussion started: 14 August 2026

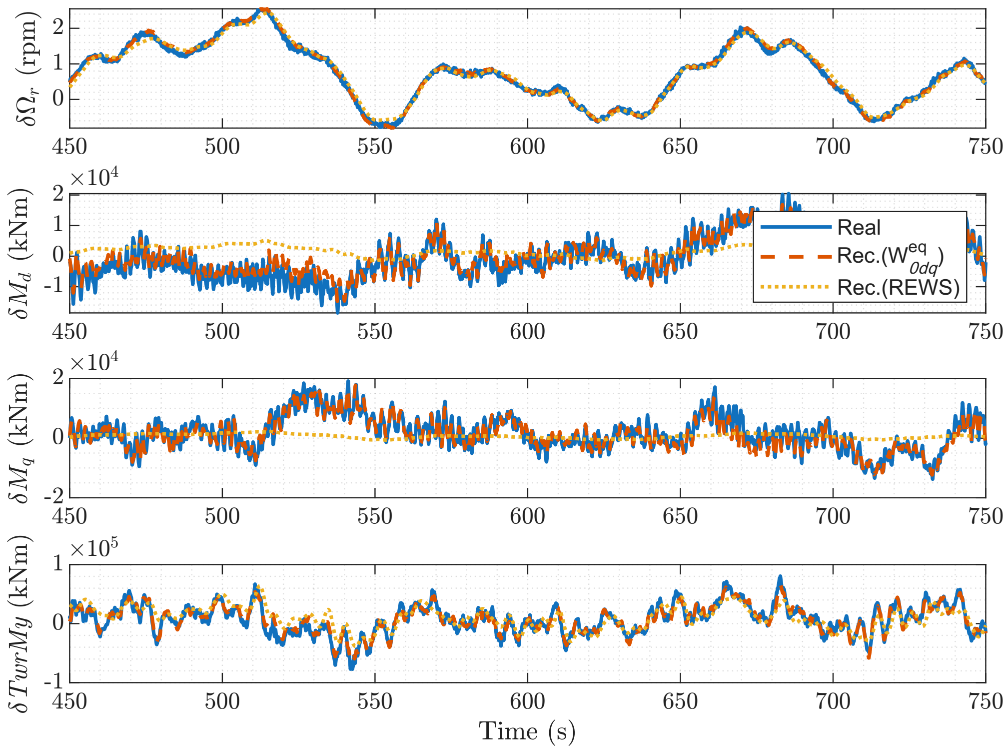

Figure 7. Comparison between simulated (solid blue) and reconstructed signals using the proposed equivalent disturbance framework (red dashed) and the REWS disturbance representation (yellow dashed) for rotor speed ($\delta\Omega_r$), tilt and yaw moments (δM_d and δM_q), and tower-base bending moment (δ*TwrMy*).

Table 1. R^2 and *NRMSE* (%) values obtained from the time-domain validation for rotor speed Ω_r, tilt moment M_d, yaw moment M_q and tower-base bending moment *TwrMy*. Metrics are reported for both the *REWS* representation and the proposed equivalent disturbance framework $\left(W^{eq}_{0dq}\right)$, as mean ± standard deviation ($\mu \pm \sigma$) over 10 turbulent simulations.

Output	$\mathbf{R}^2$ (*REWS*)	$\mathbf{R}^2$ $\left(W^{eq}_{0dq}\right)$	***NRMSE* (%)** (*REWS*)	***NRMSE* (%)** $\left(W^{eq}_{0dq}\right)$
Ω_r	0.984 ± 0.002	0.996 ± 0.001	2.096 ± 0.164	1.027 ± 0.034
M_d	—	0.928 ± 0.004	—	3.539 ± 0.275
M_q	—	0.947 ± 0.004	—	3.187 ± 0.140
TwrMy	0.615 ± 0.023	0.943 ± 0.004	8.022 ± 0.672	3.077 ± 0.219

Table 1 summarizes the mean (μ) and standard deviation (σ) of both metrics. The results show high reconstruction accuracy for all analyzed outputs, with R^2 values above 0.92 and *NRMSE* values below 4%. This confirms that the three equivalent disturbances, together with the reduced-order LTI model, capture the dominant response of the turbine under distributed turbulent inflow.

https://doi.org/10.5194/wes-2026-134
Preprint. Discussion started: 14 August 2026

For the rotor speed Ω_r, both the proposed framework and the conventional REWS-based representation provide accurate reconstructions, as this variable is predominantly driven by the collective inflow. In contrast, *TwrMy* is reproduced significantly more accurately by the proposed methodology, indicating that asymmetric inflow effects make a relevant contribution to this response.

The reconstruction metrics obtained for M_d and M_q using the REWS-based representation are not reported in Table 1, as the resulting errors are excessively large and therefore not meaningful for comparison with the remaining results. This behavior is expected, since a single collective disturbance does not contain the information required to represent the asymmetric inflow mechanisms driving these responses. These results illustrate the limitations of conventional equivalent wind speed representations when dealing with asymmetric loads and motivate the proposed framework.

4.4 Closed-loop spectral validation

The final validation step assesses whether the proposed framework can predict the closed-loop spectral response of the controlled turbine. For this purpose, a baseline control architecture composed of rotor speed regulation and conventional IPC is considered.

Rotor speed is regulated through a collective pitch controller $C_\Omega(s)$ defined as

$$C_\Omega(s) = \frac{-0.0226(s+0.6341)}{s(s+2)}, \tag{16}$$

while the IPC loop acts on the fixed-frame asymmetric load components M_d and M_q to reduce the corresponding tilt and yaw loads. In this work, identical controllers are used in both axes, such that the same control law is applied to the d and q channels. To assess the proposed methodology under different closed-loop dynamics, two IPC configurations are considered,

$$C_{d_1}(s) = C_{q_1}(s) = \frac{-8.6\times10^{-6}}{s(s+12.57)}, \quad C_{d_2}(s) = C_{q_2}(s) = \frac{-8.6\times10^{-7}}{s(s+12.57)}, \tag{17}$$

denoted as IPC_1 and IPC_2, respectively.

The resulting closed-loop system is represented by the augmented block diagram shown in Figure 8, where the three equivalent disturbances $\{\delta W_0^{eq}, \delta W_d^{eq}, \delta W_q^{eq}\}$ are explicitly introduced as external inputs. This MIMO representation captures the propagation of collective and asymmetric wind disturbances to the controlled outputs.

Based on this representation, the PSDs of the equivalent disturbances, characterized in Section 4.2, are propagated through the corresponding closed-loop transfer functions. This approach assumes that the statistical properties of the equivalent disturbances remain unchanged across the considered control configurations (Shan, 2017).

Let $\mathbf{G}(j\omega) \in \mathbb{C}^{q\times3}$ denote the closed-loop transfer matrix from the equivalent disturbances to the selected outputs. The output spectral matrix is estimated as

$$\mathbf{S}_{yy}(\omega) = \mathbf{G}(j\omega)\mathbf{S}_{ww}(\omega)\mathbf{G}^H(j\omega), \tag{18}$$

where $\mathbf{S}_{ww}(\omega) \in \mathbb{R}^{3\times3}$ is the spectral matrix of the equivalent disturbances and $(\cdot)^H$ denotes the Hermitian transpose (Ljung, 1987). In this work, the equivalent disturbances are assumed to be statistically independent, leading to

$$\mathbf{S}_{ww}(\omega) = \text{diag}\left(S_{00}(\omega), S_{dd}(\omega), S_{qq}(\omega)\right), \tag{19}$$

https://doi.org/10.5194/wes-2026-134
Preprint. Discussion started: 14 August 2026

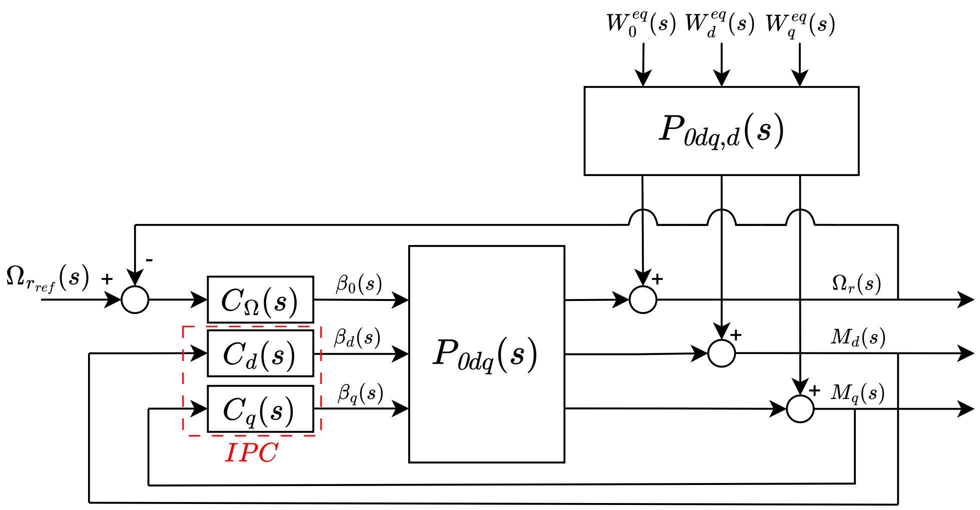

Figure 8. Augmented diagram block including the equivalent wind disturbances, used for the spectral propagation and output estimation, and proposed for advanced control designs. The perturbation notation (δ) is omitted for readability, although all signals represent deviations with respect to the operating point.

where $S_{00}(\omega)$, $S_{dd}(\omega)$ and $S_{qq}(\omega)$ are the auto-spectra of δW_0^{eq}, δW_d^{eq} and δW_q^{eq}, respectively.

Figure 9 compares the PSDs of the system outputs obtained from nonlinear closed-loop OpenFAST simulations with those estimated using (18). Results are shown for the two closed-loop configurations IPC_1 (top row) and IPC_2 (bottom row). The proposed framework accurately captures the main spectral characteristics of all considered outputs, whereas the REWS-based representation only provides satisfactory estimates for rotor speed.

To quantify the spectral prediction accuracy, the standard deviation σ_y of each signal is computed from both the nonlinear simulations and the estimated PSDs. For the simulated signals, it is obtained directly from the time domain data while for the estimated signals, the standard deviation is computed from the corresponding PSD as

$$\sigma_y = \sqrt{\frac{1}{2\pi}\int_0^\infty S_{yy}(\omega)d\omega}. \quad (20)$$

Table 2 compares the resulting standard deviations. The absolute relative errors of the proposed framework remain below 9% for all outputs and control configurations, demostrating a good agreement between the estimated and simulated variability of the signals. The load components M_d and M_q show slightly larger errors mainly due to the small underestimation of the spectral content around the *3P* region. This effect is particularly noticeable for the IPC_1 configuration, where the controller achieves a stronger reduction of the low-frequency load variability. As a consequence, the contribution of the remaining *3P* component becomes relatively more significant, increasing its impact on the estimated standard deviation and leading to a larger relative error. Nevertheless, the predicted values remain in good agreement with the nonlinear simulations.

https://doi.org/10.5194/wes-2026-134
Preprint. Discussion started: 14 August 2026

WIND ENERGY SCIENCE DISCUSSIONS

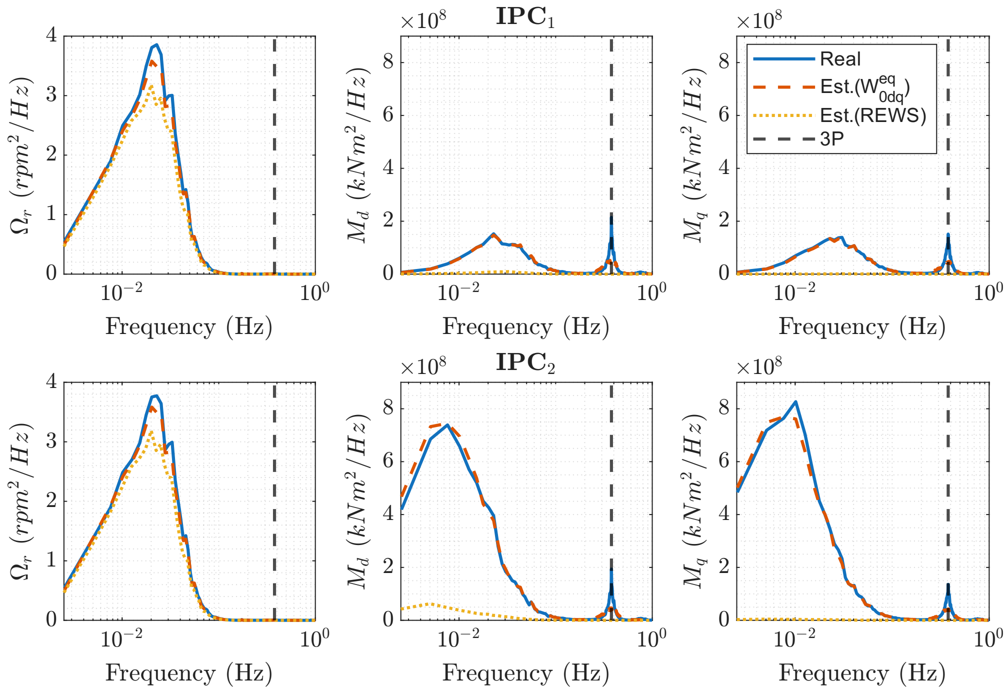

Figure 9. Comparison of simulated (blue) and estimated PSDs obtained using the proposed equivalent disturbance framework W^{eq}_{0dq} (red dashed) and REWS-based representation (yellow dotted) for Ω_r, M_d and M_q under two closed-loop configurations, IPC$_1$ (top row) and IPC$_2$ (bottom row).

Table 2. Comparison between the standard deviations obtained from nonlinear simulations (real) and those estimated using the proposed spectral framework (est.) for M_d, M_q and rotor speed Ω_r, under two closed loop configurations (IPC$_1$ and IPC$_2$).

Output	Control Loop	σ Real	σ (*REWS*)	|Rel. error| (%)	σ (W^{eq}_{0dq})	|Rel. error| (%)
Ω_r (rpm)	IPC$_1$	0.363	0.328	9.565	0.353	2.762
	IPC$_2$	0.361	0.328	9.241	0.352	2.418
M_d (kNm)	IPC$_1$	4.307e+03	—	—	3.928e+03	8.806
	IPC$_2$	5.406e+03	—	—	5.166e+03	4.430
M_q (kNm)	IPC$_1$	4.103e+03	—	—	3.780e+03	7.872
	IPC$_2$	5.361e+03	—	—	5.093e+03	4.996

For rotor speed Ω_r, the proposed framework achieves errors below 3% for both control configurations. Although the conventional REWS-based representation also provides reasonable estimates of the rotor spped variability, its errors remain around 9%. This improvement can be attributed not only to the sensitivity-based aggregation employed in the proposed framework,

https://doi.org/10.5194/wes-2026-134
Preprint. Discussion started: 14 August 2026

but also to the fact that the equivalent disturbances are constructed from the wind velocities acting directly on the blade nodes, whereas REWS is defined as a spatial average over the entire rotor disk.

These results confirm that the proposed framework can accurately estimate closed-loop output spectra by combining the characterized equivalent disturbance PSDs with the corresponding closed-loop transfer functions. The framework establishes a direct link between the characteristics of the inflow disturbances and the resulting system response, allowing control strategies to be evaluated in terms of the disturbances they are intended to reject. This leads to a more transparent and systematic control design workflow while reducing the dependence on computationally expensive aeroelastic time-domain.

5 Conclusions and Future Work

This work has presented a unified control-oriented framework that combines the modeling and characterization of equivalent wind disturbances in the *0dq* reference frame. Starting from a linearized model with distributed horizontal wind inputs, the proposed methodology reduces the high-dimensional inflow description to three physically meaningful disturbances associated with the collective, tilt and yaw components of the wind field.

The framework has been validated both in the time and frequency domains. In the time domain, the reduced-order model driven by the equivalent disturbances accurately reproduces the main turbine responses obtained from nonlinear aeroelastic simulations. In the frequency domain, the spectral characterization of the equivalent disturbances, combined with closed-loop transfer functions, enables the estimation of the output PSDs under different control configurations.

The main contribution of the proposed approach is that it explicitly incorporates both the turbine model and the characterization of the disturbances affecting the system outputs. As a result, asymmetric load reduction strategies can be designed in a more systematic way, since the required control design effort can be directly related to the spectral content of the disturbances to be rejected. This provides a more transparent and consistent control design workflow than approaches based only on output response simulations or uncharacterized disturbance inputs.

Moreover, these findings confirm that the proposed approach enables a consistent prediction of closed-loop system behavior using a reduced-order linear model, effectively separating the inflow characterization from the control-dependent dynamics. This provides a computationally efficient alternative to simulation-based analysis and facilitates the evaluation of control strategies from a spectral perspective. In addition, the availability of closed-loop output spectra enables the formulation of advanced control specifications directly in the frequency domain, such as fatigue-based or actuator-usage specifications (see e.g. (Miquelez-Madariaga et al., 2026; Lacheta-Lecumberri et al., 2026)).

Future work will focus on exploiting the proposed framework for advanced control design based on frequency domain specifications, with methodologies such as Quantitative Feedback Theory (QFT) or H_∞. In this context, the equivalent disturbance spectra could be used to define disturbance-rejection requirements, load-reduction objectives and actuator-effort constraints in a unified frequency-domain design framework.

https://doi.org/10.5194/wes-2026-134
Preprint. Discussion started: 14 August 2026

Author contributions. DLL: Conceptualization, formal analysis, methodology, validation, visualization, writing (original draft preparation). IMM: Conceptualization, writing (review and editing). JE: Conceptualization, writing (review and editing).

Competing interests. The authors declare that they have no conflict of interest.

Acknowledgements. The authors grategully appreciate the support given by the Government of Navarre through the *Doctorados Industriales 2023* grant program number [0011-1408-2023-000013].

https://doi.org/10.5194/wes-2026-134
Preprint. Discussion started: 14 August 2026

References

Bertelè, M., Bottasso, C. L., Cacciola, S., Daher Adegas, F., and Delport, S.: Wind inflow observation from load harmonics, Wind Energy Science, 2, 615–640, https://doi.org/10.5194/wes-2-615-2017, 2017.

Bertelè, M., Meyer, P. J., Sucameli, C. R., Fricke, J., Wegner, A., Gottschall, J., and Bottasso, C. L.: The rotor as a sensor – observing shear and veer from the operational data of a large wind turbine, Wind Energy Science, 9, 1419–1429, https://doi.org/10.5194/wes-9-1419-2024, 2024.

Bir, G.: Multi-Blade Coordinate Transformation and its Application to Wind Turbine Analysis, in: 46th AIAA Aerospace Sciences Meeting and Exhibit, American Institute of Aeronautics and Astronautics, Reno, Nevada, ISBN 978-1-62410-128-1, https://doi.org/10.2514/6.2008-1300, 2008.

Bossanyi, E. A.: Individual Blade Pitch Control for Load Reduction, Wind Energy, 6, 119–128, https://doi.org/10.1002/we.76, 2003.

Bottasso, C., Cacciola, S., and Schreiber, J.: Local wind speed estimation, with application to wake impingement detection, Renewable Energy, 116, 155–168, https://doi.org/10.1016/j.renene.2017.09.044, 2018.

Bošnjaković, M., Katinić, M., Santa, R., and Marić, D.: Wind Turbine Technology Trends, Applied Sciences, 12, 8653, https://doi.org/10.3390/app12178653, 2022.

Burton, T. L., Jenkins, N., and Bossanyi, E.: Wind Energy Handbook, 3rd edn., 2021.

Cacciola, S., Bertelè, M., and Bottasso, C.: Simultaneous observation of wind shears and misalignments from rotor loads, Journal of Physics: Conference Series, 753, 052 002, https://doi.org/10.1088/1742-6596/753/5/052002, 2016.

Canet, H., Bortolotti, P., and Bottasso, C. L.: On the scaling of wind turbine rotors, Wind Energy Science, 6, 601–626, https://doi.org/10.5194/wes-6-601-2021, 2021.

Dai, J., Li, M., Chen, H., He, T., and Zhang, F.: Progress and challenges on blade load research of large-scale wind turbines, Renewable Energy, 196, 482–496, https://doi.org/10.1016/j.renene.2022.07.017, 2022.

Gaertner, E., Rinker, J., Sethuraman, L., Zahle, F., Anderson, B., Barter, G., Abbas, N., Meng, F., Bortolotti, P., Skrzypinski, W., Scott, G., Feil, R., Bredmose, H., Dykes, K., Shields, M., Allen, C., and Viselli, A.: Definition of the IEA 15-Megawatt Offshore Reference Wind Turbine, https://docs.nrel.gov/docs/fy20osti/75698.pdf, 2020.

Henrique, A. I. D., Zhao, F., Backwell, B., Clarke, E., Ladwa, R., Jayasurya, F., Hutchinson, M., Williams, R., Han, W., Liang, W., Fang, E., Francisco, A. M., Shardul, M., Gitobu, J., Cheong, J., Muchiri, W., Fiestas, R., Rabie, H., Madan, K., Cargill, J., Lu, E., Sanchez, J. T., Melkonyan, N., Esteves, J., and Moreaux, B.: Global Wind Energy Council, Tech. rep., 2025.

Hummel, J. I. S., Kober, J., and Mulders, S. P.: Output-constrained individual pitch control methods using the multiblade coordinate transformation: Trading off actuation effort and blade fatigue load reduction for wind turbines, https://doi.org/10.5194/wes-2024-153, 2025.

IEC Technical Committee: IEC 61400-1 Ed 3: Wind Turbines. Part 1, Design Requirements, 2020.

Jonkman, B. J.: Turbsim User's Guide: Version 1.50, Tech. Rep. NREL/TP-500-46198, 965520, https://doi.org/10.2172/965520, 2009.

Jonkman, J., Wright, A. D., Hayman, G., and Robertson, A. N.: Full-System Linearization for Floating Offshore Wind Turbines in OpenFAST: Preprint, Tech. Rep. NREL/CP–5000-71865, 1489323, https://doi.org/10.2172/1489323, 2018.

Jonkman, J. M. and Buhl, M. L. J.: FAST User's Guide - Updated August 2005, Tech. Rep. NREL/TP-500-38230, 15020796, https://doi.org/10.2172/15020796, 2005.

Lacheta-Lecumberri, D., Miquelez-Madariaga, I., and Elso, J.: Spectral Methodology for Probabilistic Estimation of Pitch Actuator Rate Saturation in Wind Turbines, Journal of Physics: Conference Series, 3224, 052 007, https://doi.org/10.1088/1742-6596/3224/5/052007, 2026.

Laks, J., Pao, L., Wright, A., Kelley, N., and Jonkman, B.: Blade Pitch Control with Preview Wind Measurements, in: 48th AIAA Aerospace Sciences Meeting Including the New Horizons Forum and Aerospace Exposition, American Institute of Aeronautics and Astronautics, Orlando, Florida, ISBN 978-1-60086-959-4, https://doi.org/10.2514/6.2010-251, 2010.

Lara, M., Ruz, M. L., Mulders, S. P., Vázquez, F., and Garrido, J.: Individual pitch controller with static inverted decoupling for periodic blade load reduction on monopile offshore wind turbines, Ocean Engineering, 334, 121 608, https://doi.org/10.1016/j.oceaneng.2025.121608, 2025.

Ljung, L.: System Identification: Theory for the User, Prentice Hall PTR, 2nd edn., ISBN 0-13-656695-2, 1987.

Miquelez-Madariaga, I., Lizarraga-Zubéldia, I., Diaz De Corcuera, A., and Elso, J.: Linear uncertain modelling of LIDAR systems for robust wind turbine control design, Renewable Energy, 206, 367–374, https://doi.org/10.1016/j.renene.2023.02.062, 2023.

Miquelez-Madariaga, I., Arellano, J., Lacheta-Lecumberri, D., and Elso, J.: Design of fatigue-based specifications for the design of controllers in wind turbines, Wind Energy Science, 11, 405–416, https://doi.org/10.5194/wes-11-405-2026, 2026.

Miquelez-Madariaga, I., Lizarraga-Zubeldia, I., Diaz De Corcuera, A., and Elso, J.: Lidar-based feedforward control design methodology for tower load alleviation in wind turbines, Wind Energy, 25, 1238–1251, https://doi.org/10.1002/we.2724, 2022.

Park, R. H.: Two-reaction theory of synchronous machines generalized method of analysis-part I, Transactions of the American Institute of Electrical Engineers, 48, 716–727, https://doi.org/10.1109/T-AIEE.1929.5055275, 1929.

Schlipf, D.: Prospects of a collective pitch control by means of predictive disturbance compensation assisted by wind speed measurements, 2008.

Schlipf, D., Cheng, P. W., and Mann, J.: Model of the Correlation between Lidar Systems and Wind Turbines for Lidar-Assisted Control, Journal of Atmospheric and Oceanic Technology, 30, 2233–2240, https://doi.org/10.1175/JTECH-D-13-00077.1, 2013.

Selvam, K., Kanev, S., Van Wingerden, J. W., Van Engelen, T., and Verhaegen, M.: Feedback–feedforward individual pitch control for wind turbine load reduction, International Journal of Robust and Nonlinear Control, 19, 72–91, https://doi.org/10.1002/rnc.1324, 2009.

Shan, M.: Load Reducing Control for Wind Turbines: Load Estimation and Higher Level Controller Tuning based on Disturbance Spectra and Linear Models, Ph.D. thesis, University of Kassel, https://kobra.uni-kassel.de/items/a52780db-576e-4d0f-b256-1da2ad06c981, 2017.

Simley, E. and Pao, L.: Correlation between Rotating LIDAR Measurements and Blade Effective Wind Speed, in: 51st AIAA Aerospace Sciences Meeting including the New Horizons Forum and Aerospace Exposition, American Institute of Aeronautics and Astronautics, Grapevine (Dallas/Ft. Worth Region), Texas, ISBN 978-1-62410-181-6, https://doi.org/10.2514/6.2013-749, 2013.

Stol, K., Moll, H.-G., Bir, G., and Namik, H.: A Comparison of Multi-Blade Coordinate Transformation and Direct Periodic Techniques for Wind Turbine Control Design, in: 47th AIAA Aerospace Sciences Meeting including The New Horizons Forum and Aerospace Exposition, American Institute of Aeronautics and Astronautics, Orlando, Florida, ISBN 978-1-60086-973-0, https://doi.org/10.2514/6.2009-479, 2009.

Tang, S., Tian, D., Wu, X., Huang, M., and Deng, Y.: Wind turbine load reduction based on 2DoF robust individual pitch control, Renewable Energy, 183, 28–40, https://doi.org/10.1016/j.renene.2021.10.086, 2022.

Trigaux, F., Chatelain, P., and Winckelmans, G.: Impact of rotor size on the aeroelastic behavior of large turbines: a LES study using flexible actuator lines, Journal of Physics: Conference Series, 2767, 022 062, https://doi.org/10.1088/1742-6596/2767/2/022062, 2024.

https://doi.org/10.5194/wes-2026-134
Preprint. Discussion started: 14 August 2026

Yuan, Y., Chen, X., and Tang, J.: Multivariable robust blade pitch control design to reject periodic loads on wind turbines, Renewable Energy, 146, 329–341, https://doi.org/10.1016/j.renene.2019.06.136, 2020.